



Crystal chemistry of ferriallanite-(Ce) from Nya Bastnäs, Sweden: Chemical and spectroscopic study

Kamil Sobek¹ · Zdeněk Losos¹ · Radek Škoda¹ · Markéta Holá² · Lutz Nasdala³

Received: 9 November 2022 / Accepted: 14 April 2023 / Published online: 13 May 2023
© The Author(s) 2023

Abstract

A second study of ferriallanite-(Ce) from Nya Bastnäs, Sweden, extends current data by using electron probe micro-analysis (EPMA), laser ablation inductively coupled plasma mass spectrometry (LA-ICP-MS) analysis and brings new insights about its crystal chemistry obtained by Raman spectroscopy. The study presents the first Raman spectra for ferriallanite-(Ce) member of the allanite group (not considering the rather low-quality spectra published in preceding papers). The material does not show significant radiation damage, which is rare as allanite-group minerals often have undergone metamictisation due to significant amounts of incorporated radionuclides (U, Th). Some interior regions show pronounced zoning that correlates with variations in Raman-band positions. In spite of its significant REE content, the material is virtually non-luminescent. New additional data for allanite-(Ce) from Oßling, Germany and Domanínek, Czech Republic are also presented, which were used for comparison.

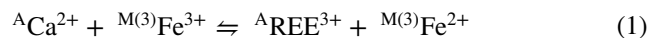
Keywords Allanite group · Raman spectroscopy · EPMA · LA-ICP-MS · Bastnäs (Sweden) · Deposit · Crystal chemistry

Introduction

Ferriallanite-(Ce) is a mineral belonging to the allanite group of the epidote supergroup. The general crystal chemical formula is $A(1)A(2)M(1)M(2)M(3)(SiO_4)(Si_2O_7)O(OH)$, where A represents a 9- or 11-coordinated polyhedral site mostly occupied by Ca, lanthanoids (Ln), Y, Th, U^{4+} and Mn^{2+} and M are octahedral sites mostly occupied by Al, Fe^{3+} and Fe^{2+} . Silicon occurs in isolated SiO_4 tetrahedra and Si_2O_7 groups (Fig. 1). Minerals of the epidote supergroup are monoclinic, space group $P2_1/m$. Various solid solutions exist among endmembers, which are based on elemental substitutions in A and/or M positions (Dollase 1971; Bonazzi and

Menchetti 1995; Gieré and Sorensen 2004; Armbruster et al. 2006; see Table 1).

The most common compositional relationships in the allanite-ferriallanite-epidote-clinozoisite solid solution can be expressed via the following substitutional vectors:



These relationships can be depicted in a ΣREE versus Al diagram for such solid solutions proposed by Petrík et al. (1995), which also allows one to estimate the Fe^{2+}/Fe^{3+} ratio. However, other substitutions involving Mn^{2+} , Mn^{3+} , Mg, Pb^{2+} , V, Cr, Ti, Sn, Sc and others are possible as well (Dollase 1969; Grew et al. 1991; Bonazzi and Menchetti 2004; Ahijado et al. 2005; Miyawaki et al. 2008; Nagashima et al. 2013; Biagioni et al. 2019). The possibility of F^- substituting for O^{2-} in epidote-supergroup minerals has been reported as well (Peacor and Dunn 1988), but its extent tends to be generally low except from minerals of the dollaseite group (Pautov et al. 1993; Ercit 2002).

The crystal structure of both allanite-(Ce) and ferriallanite-(Ce) are almost identical to that of other epidote-group minerals (Ueda 1955; Dollase 1971; Franz and Liebscher 2004; Gieré and Sorensen 2004). A(1) is normally occupied

Editorial handling: E. Libowitzky

✉ Kamil Sobek
sobekk@mail.muni.cz

¹ Department of Geological Sciences, Faculty of Science, Masaryk University, Kotlářská 267/2, 611 37 Brno, Czech Republic

² Department of Chemistry, Faculty of Science, Masaryk University, Kamenice 753/5, 625 00 Brno, Czech Republic

³ Institut für Mineralogie und Kristallographie, Universität Wien, Josef-Holaubek-Platz 2, 1090 Vienna, Austria

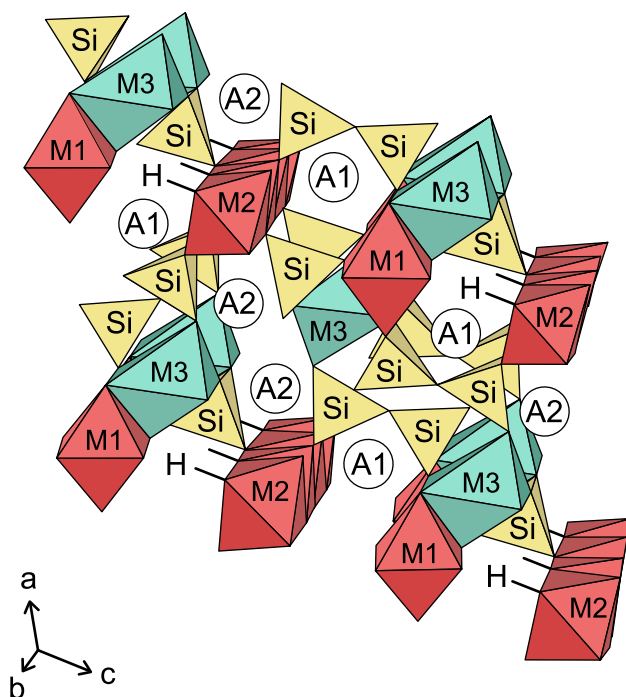


Fig. 1 Sketch of the crystal structure of allanite-group minerals. It consists of chains of edge-sharing M(1) octahedra and edge-sharing M(2) octahedra (red). These chains are linked by SiO_4 tetrahedra and Si_2O_7 groups (yellow). Slightly deformed M(3) octahedra are shown turquoise. Large cavities in the framework belong to A(1) and A(2) polyhedra where elements such as Ca^{2+} or REE^{3+} are present in ninefold and 11-fold coordination to oxygen, respectively. Hydrogen atoms are marked “H”. Sketch based on Dollase (1971) and Reissner et al. (2019), drawn with the JP-Minerals VESTA v3 software (Momma and Izumi 2011)

by ninefold coordinated Ca, however, the polyhedron's uneven shape causes the coordination number to range from 7 to 11. The A1 and A2 sites are best represented as being ninefold and tenfold coordinated, respectively. For the allanites A(2) position is 11-fold coordinated and occupied by REE^{3+} ; individual mineral species are distinguished based on the dominating REE (Ercit 2002; Armbruster et al. 2006). Although Fe^{3+} occurs partitioned over the M(1) and M(3) octahedral sites in all iron-rich epidote supergroup minerals, it is the dominant cation at the M(1) position in ferriallanites, ferriandrosites and ferriakasakaite (Dollase 1973; Nozik et al. 1978; Kvik et al. 1988; Franz and Liebscher 2004; Gieré and Sorensen 2004; Nagashima et al. 2013). The distorted, large M(3) octahedron accommodates almost all of the Fe^{2+} ; however, some Fe^{2+} may also occur in the M(1) site (Dollase 1973; Kartashov et al. 2003). Among all epidote-supergroup minerals, Fe^{2+} is an essential constituent in allanite, ferriallanite, vanadoallanite and uedaite where the presence of Fe^{2+} contributes to an increased unit-cell volume and affects optical properties. According to Kartashov et al. (2003), ferriallanite-(Ce) has the largest unit cell of all REE-rich minerals belonging to the epidote supergroup.

The radionuclides Th and U readily enter the crystal structure of allanite-group minerals, owing to their similar ionic radii with those of REE. The radioactive decay of Th and U causes structural damage. Even minor amounts of radionuclides may thus lead to a transformation from the crystalline to a glassy state over geological periods of time; such glassy state is referred to as metamict (Ewing 1994). Metamict minerals generally have lowered chemical resistance

Table 1 Idealized formulae of selected members of the epidote supergroup, following the nomenclature of Armbruster et al. (2006) and Varlamov et al. (2019)

Structural position	A(1)	A(2)	M(1)	M(2)	M(3)	T	O(4)	
Epidote group:								
Clinozoisite	Ca^{2+}	Ca^{2+}	Al^{3+}	Al^{3+}	Al^{3+}	Si_3O_{11}	O	OH
Epidote	Ca^{2+}	Ca^{2+}	Al^{3+}	Al^{3+}	Fe^{3+}	Si_3O_{11}	O	OH
Piemontite	Ca^{2+}	Ca^{2+}	Al^{3+}	Al^{3+}	Mn^{3+}	Si_3O_{11}	O	OH
Allanite group:								
Allanite	Ca^{2+}	REE^{3+}	Al^{3+}	Al^{3+}	Fe^{2+}	Si_3O_{11}	O	OH
Ferriallanite	Ca^{2+}	REE^{3+}	Fe^{3+}	Al^{3+}	Fe^{2+}	Si_3O_{11}	O	OH
Vanadoallanite	Ca^{2+}	REE^{3+}	V^{3+}	Al^{3+}	Fe^{2+}	Si_3O_{11}	O	OH
Dissakisite	Ca^{2+}	REE^{3+}	Al^{3+}	Al^{3+}	Mg^{2+}	Si_3O_{12}	O	OH
Ferriakasakaite	Ca^{2+}	REE^{3+}	Fe^{3+}	Al^{3+}	Mn^{2+}	Si_3O_{12}	O	OH
Androsite	Mn^{2+}	REE^{3+}	Al^{3+}	Al^{3+}	Mn^{2+}	Si_3O_{11}	O	OH
Ferriandrosite	Mn^{2+}	REE^{3+}	Fe^{3+}	Al^{3+}	Mn^{2+}	Si_3O_{11}	O	OH
Uedaite	Mn^{2+}	REE^{3+}	Al^{3+}	Al^{3+}	Fe^{2+}	Si_3O_{11}	O	OH
Dollaseite group								
Dollaseite	Ca^{2+}	REE^{3+}	Mg^{2+}	Al^{3+}	Mg^{2+}	Si_3O_{11}	F	OH
Khristovite	Ca^{2+}	REE^{3+}	Mg^{2+}	Al^{3+}	Mn^{2+}	Si_3O_{11}	F	OH
Åskanenite group:								
Åskagenite	Mn^{2+}	REE^{3+}	Al^{3+}	Al^{3+}	Fe^{3+}	Si_3O_{11}	O	O

and are more susceptible to secondary alteration processes, compared to their crystalline counterparts. This is especially true for fluid-driven chemical alteration that may result in substantial compositional changes (Gieré and Sorensen 2004; Bonazzi et al. 2009). The accumulation of radiation damage also causes changes of physical properties, such as volume expansion that is detected from shifts of X-ray diffraction maxima to lower 2θ values (Ewing et al. 1987; Janeczek and Eby 1993; Reissner et al. 2019). Decrease of the short-range order may be detected using Raman spectroscopy. For instance, Raman spectra of radiation-damaged natural zircon show increased band broadening accompanied by band downshifts, depending on the self-irradiation dose. In some cases, band broadening can be used to estimate the degree of radiation damage, provided significant band broadening due to chemical variations is excluded (Nasdala et al. 1995).

Allanite-group minerals are common accessory phases in granitic pegmatites, granites, granodiorites, syenites, diorites, etc. (e.g., Dollase 1971, 1973; Deer et al. 1986; Broska et al. 2000). They can also occur in various metamorphic rocks, especially metasomatic rocks (Deer et al. 1986; Sorensen 1991; Wing et al. 2003) and skarns. The Nya Bastnäs deposit located in Skinnskatteberg, Bergslagen ore region, Sweden, belongs to the Bastnäs-type Fe-REE deposits. Here, typical Fe skarn hosts pods or layers of massive REE mineralisation. The dominant host rock is a metasomatized volcanic rock interlayered with rocks dominated by quartz, occurring adjacent to ore bodies (Holtstam et al. 2014). The allanite-group minerals are assumed to be of metasomatic origin (Andersson 2004; Holtstam et al. 2014; Sahlström et al. 2019). Initially exploited as a source of Cu and Fe, this deposit, in the nineteenth century, became a significant source of REE ores, with cerite-(Ce), bastnäsite-(Ce) and other REE-rich phases (Holtstam et al. 2003; Andersson, 2004). Other minerals described from this locality are tremolitic amphibole, accessory sulphides and oxides such as chalcopyrite, bismuthine, molybdenite and magnetite. In some rare cases uraninite is present locally (Holtstam and Ensterö 2002; Ensterö 2003; Andersson 2004). The specimen investigated in the present study (Fig. 2) originates from a massive REE mineralisation consisting of epidote-superfgroup minerals and minor gadolinite-(Nd) in actinolite-tremolite matrix.

The main aim of the present study was to expand our knowledge regarding crystal-chemical characteristics of allanite-group minerals. To the best of our knowledge, no detailed spectroscopic studies of ferriallanites samples have been undertaken thus far, and the only spectra of ferriallanite-(La) that have been published are of rather low quality (Varlamov et al. 2019). To provide some rationale for the relationship between Raman spectra and composition, the combination of Raman spectroscopy with EPMA was chosen as main tools. To provide basic information about the



Fig. 2 A specimen containing ferriallanite-(Ce), as a dark brown to black layer up to 3 cm wide, in contact with greenish-white, fibrous amphibole and newly formed weathering products around the edges, from Nya Bastnäs, Sweden. Photo by Kamil Sobek

relative changes of elements distribution in the sample, LA-ICP-MS served as a supplementary method to visualise such changes in the form of qualitative maps. Also, REE-bearing minerals often show distinct luminescence that may be used as a helpful fingerprinting tool for mineral identification. The photoluminescence-based detection of allanite-(Ce) may be possible based on the Nd^{3+} emission in the near-infrared range (about $10,600\text{--}11,900\text{ cm}^{-1}$; see for instance Lenz et al. 2015; Zeug et al. 2017). Therefore, laser-induced photoluminescence (PL) was also included.

Materials and methods

Samples and preparation

We have investigated a 6 cm long specimen of ferriallanite-(Ce) layer in amphibole matrix originating from a mine dump near Nya Bastnäs, Skinnskatteberg area, Sweden (Fig. 2). Two other samples were studied as references for comparison, metamict allanite-(Ce) from a pegmatite near Domanínek in Czech Republic (Čermák 2013) and acicular, well-crystallized allanite-(Ce) of hydrothermal origin from Obting, Germany (Nasdala 1993). The Bastnäs specimen was cut into several polished sections ($100\text{ }\mu\text{m}$ thickness) and attached to a glass slide. Some fragments were heated in air to check for possible annealing of radiation damage. For this, the fragments were placed in a Pt crucible and heated to $280\text{ }^{\circ}\text{C}$ at a rate of $30\text{ }^{\circ}\text{C}/\text{min}$. At the end of a 96-h run, the furnace was switched off and the sample was allowed to cool to below $50\text{ }^{\circ}\text{C}$ before taken out of the oven. Reference samples were also embedded in epoxy and polished. For EPMA analysis, samples were coated with carbon.

EPMA

Chemical spot analyses, line scans and back-scattered electron (BSE) images were obtained using a CAMECA SX-100 system operated in wavelength-dispersive X-ray spectrometry mode. The accelerating voltage was 15 kV, the beam current 20 nA, and the focal spot of the electron beam had a diameter of 2 μm . The following natural and synthetic materials (analysed X-ray line in parentheses) were used for calibration: Ti ($K\alpha$)—anatase; Fe ($K\alpha$)—almandine; Mn ($K\alpha$)—rhodonite; Ca, Si ($K\alpha$)—wollastonite, Na ($K\alpha$)—albite; P ($K\alpha$)— $\text{Ca}_5(\text{PO}_4)_3\text{F}$; Al ($K\alpha$)—sanidine; Mg ($K\alpha$)— Mg_2SiO_4 ; F ($K\alpha$)—topaz, Cl ($K\alpha$)—vanadinite; Y ($L\alpha$)—YAG; Zr ($L\alpha$)— ZrSiO_4 ; La, Ce ($L\alpha$); Pr, Nd, Sm, Gd, ($L\beta$)—individual La–Yb orthophosphates. Peak counting times (same as their background counting times) varied from 10 to 100 s depending on the element. Raw X-ray intensities were processed for matrix corrections using X-PHI algorithm of Merlet (1994). An empirically determined correction factor was applied to the coincidence of the 2nd order of Ce– $M\beta$ with the $FK\alpha$ line, Ce– $L\gamma$ with the Tm– $L\alpha$, and with the Yb– $L\alpha$ line. In addition, Na_2O , Sc_2O_3 , P_2O_5 , SnO_2 , ThO_2 , UO_2 , Dy_2O_3 , Ho_2O_3 , Er_2O_3 , ZrO_2 , Eu_2O_3 , Tm_2O_3 , Yb_2O_3 , Lu_2O_3 and PbO were sought but their contents were below the EPMA detection limits.

LA-ICP-MS

LA-ICP-MS analyses were performed by using a pulsed Nd:YAG laser system LSX-213 G2 + working at 213 nm wavelength and using a pulse duration of ~ 4 ns. The ablation system is equipped with a 2-volume ablation cell (HelEx) designed to enable rapid eluting of the ablation-generated aerosol in a large format cell. Helium was used as a carrier gas with a flow rate of 0.9 l/min. The aerosol was transported from the ablation cell through a 1 m long FEP (Fluorinated Ethylene Propylene) transport tube (2 mm in diameter) to the ICP discharge of the quadrupole mass spectrometer ICP-MS Agilent 7900. The mass spectrometer operated at the forwarded power of 1550 W and Ar gas flow rate of 15 l/min (outer plasma gas). The analysis was performed by a set of continuous line scans using laser pulses covering a defined area of the sample to create qualitative maps. Qualitative maps were obtained with the spot diameter of 4 μm , fluence of $10 \text{ J}\cdot\text{cm}^{-2}$, scan speed of 4 $\mu\text{m}/\text{s}$ and repetition rate of 20 Hz. The following isotopes were monitored during the LA-ICP-MS scan measurements with the total integration time of 1 s: ^{24}Mg , ^{27}Al , ^{29}Si , ^{31}P , $^{43,44}\text{Ca}$, ^{55}Mn , ^{57}Fe , ^{88}Sr , ^{89}Y , ^{90}Zr , $^{139-159}\text{Ln}$, ^{232}Th , ^{238}U . Data were processed in ILaps by Faltusová et al. (2022).

Raman and photoluminescence spectroscopy

Raman and PL spectra, including line scans, were obtained at room temperature by means of a Horiba Jobin Yvon LabRam-HR Evolution. The system was equipped with an Olympus BX41 optical microscope, a Si-based, Peltier-cooled charge-coupled device detector, and a diffraction grating with 1800 grooves per millimetre. Spectra were excited with the 473 nm emission of a diode laser (10.5 mW at the sample surface). Attempts to obtain PL spectra were also made with 532, 633 and 785 nm laser excitation. The instrument was calibrated using the Rayleigh line, resulting in a wavenumber accuracy of 0.5 cm^{-1} . An Olympus 100 \times objective (numerical aperture 0.90) was used. Spectra were obtained in a range 110–4000 cm^{-1} in confocal mode; the lateral resolution was better than 1 μm . The spectral resolution was better than 1.2 cm^{-1} . Line scans were done using an automated, software-controlled x–y stage. All spectra were obtained in areas about 10 μm away from EPMA points (to avoid unwanted effects of the electron-beam impact). Band fitting was done after appropriate background correction, assuming Lorentzian-Gaussian band shapes.

Results

General description

Ferriallanite-(Ce) from Nya Bastnäs shows irregular zoning, which is even visible by the unaided eye. When observed in plane-polarised transmitted light, a wide range of colour sectors (ranging from light green to dark brown) with intensive pleochroism are seen. In cross-polarised transmitted light, these sectors have high second-order interference colours that are, however, widely masked by body colour (Fig. 3).

Crystal chemistry

BSE imaging revealed detailed zonation patterns that reflect variations in chemical composition. Textural relations indicate that interior regions with primary growth zoning were replaced by patchily zoned domains. These domains were chosen for more detailed examination (see lines 1 and 2 in Fig. 4). Differences in BSE intensity reflect mainly the variation of Ca (9.5–16.1 wt% of CaO) and REE (14.6–27.1 wt% of REE_2O_3), which are accompanied by changes in total Fe oxide (15.4–19.1 wt%) and Al_2O_3 (11.9–17.4 wt%). Results of chemical analyses are summarised in Table 2 (means and ranges), and all individual analysis results are provided in Tables S1–S5 in the electronic supplementary material (ESM).

Ferriallanite-(Ce) from Nya Bastnäs contains high solid solution contents of allanite and REE-rich epidote according

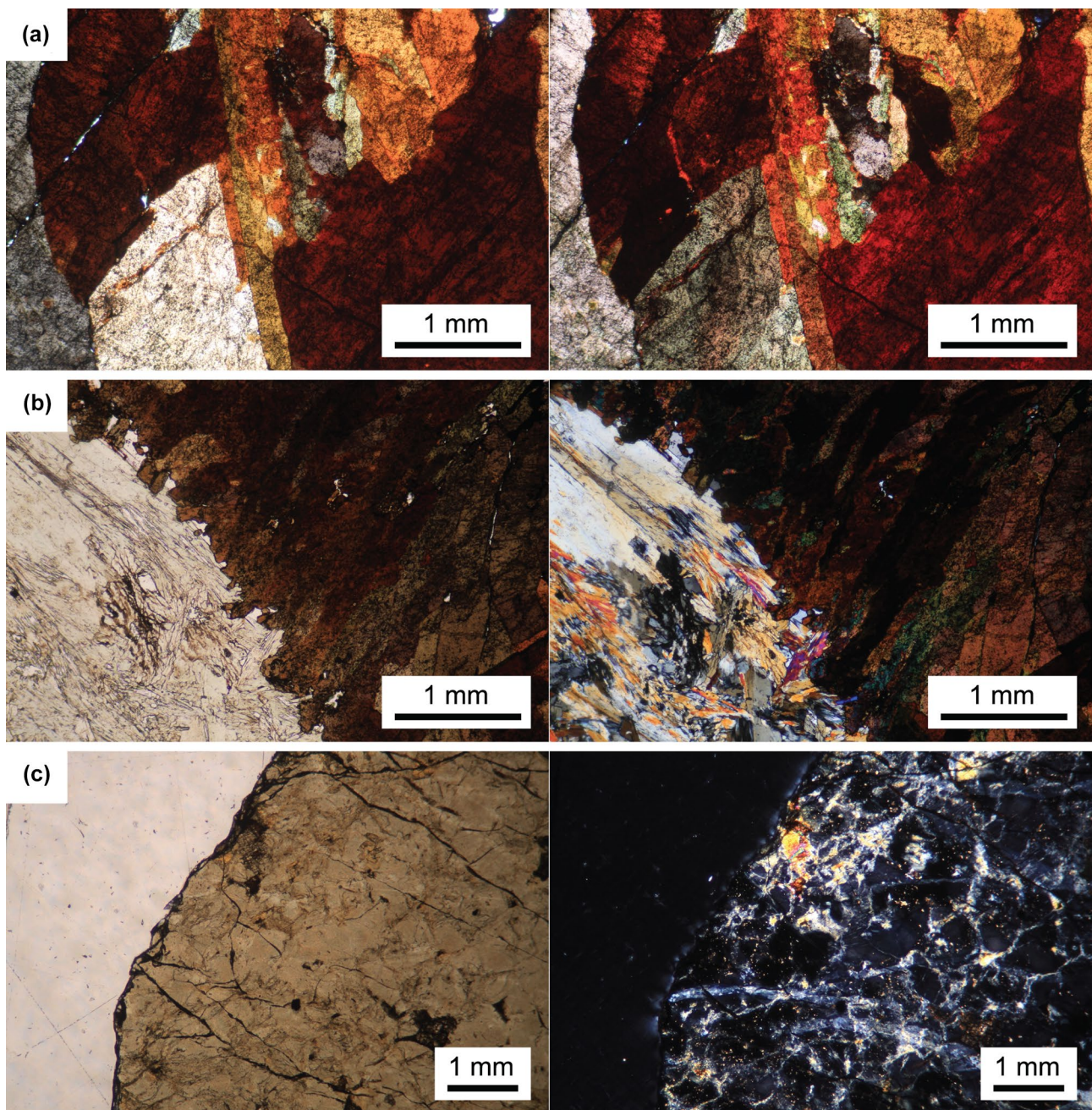


Fig. 3 Pairs of plane-polarised (left) and cross-polarised (right) transmitted-light photomicrographs. **a** Aggregate consisting of several randomly oriented ferriallanite-(Ce) crystals, originating from Nya Bastnäs. **b** Edge of the ferriallanite-(Ce) aggregate. The neighbour-

ing, acicular amphibole is seen on the lower left side. **c** This metamict allanite-(Ce) from Domanínek is shown for comparison. Note the nearly complete absence of interference colours

to the Al (Al = 1.39–1.85 apfu), Fe (1.09–1.49 apfu) and low Mg (Mg = 0.04–0.19 apfu) contents. Values show compositional variation between Fe^{3+} ($\text{Fe}^{3+} = 0.47\text{--}0.83$ apfu) and Fe^{2+} ($\text{Fe}^{2+} = 0.42\text{--}0.89$ apfu). The mineral is generally Mn- and Ti-poor (Mn 0.01–0.02 apfu, $\text{Ti} \leq 0.01$ apfu). Total REEs vary in the range 0.47–0.96 apfu. Note that concentrations of light REEs are significant, up to about

20 wt%, whereas heavy REEs were close to or even below the EPMA detection limits. This corresponds to previous observations that in allanite-group minerals, light REEs are generally enriched (Vlach and Gualda 2007; Papoutsas and Pe-Piper 2015). Based on method proposed by Armbruster et al. (2006) crystal-chemical formulae were derived by assigning cations at the individual structural sites for two

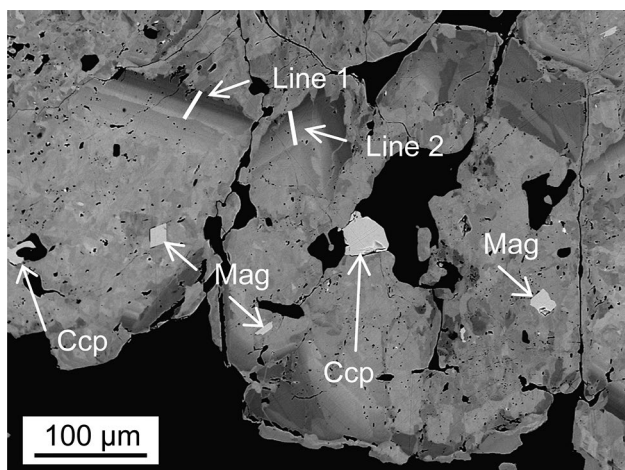


Fig. 4 BSE image of showing internal heterogeneity of ferriallanite-(Ce) from Nya Bastnäs. There are interior regions with well-developed zoning. Abbreviations of mineral names: Ccp – chalcopyrite, Mag – magnetite

extreme compositions (circles pale grey and very dark grey, see Fig. 5). The pale grey colour represents the ferriallanite-(Ce) member of the allanite subgroup according to $[M^{3+} + M^{4+}]_{A2} > 0.50$, $[M^{2+}]_{M3} > 0.50$ with formulae $A^1(Ca)_A^2(REE, Y^{3+}, Ca, Mn^{2+})M^1(Fe^{3+}, Al)^{M2}(Al)^{M3}(Fe^{2+}, Mn^{2+}, Mg, Ti)^{T1,2,3}[Si_3O_{12}](OH)$; however, the variable chemistry also shows trends towards REE-rich epidote in the dark grey areas, where the darkest circles belong to both the allanite and the clinozoisite subgroup by meeting the additional condition $[M^{2+}]_{A2} > 0.5$ with formulae $A^1(Ca)_A^2(Ca, REE, Y^{3+})M^1(Fe^{3+}, Al)^{M2}(Al)^{M3}(Fe^{2+}, Mn^{2+}, Mg, Ti, Al)^{T1,2,3}[Si_3O_{12}](OH)$. The presence of U and Th was below the detection limits of EPMA (0.09 wt% and 0.07 wt%, respectively).

Data obtained by LA-ICP-MS correlate with EPMA results, especially in REE-rich and REE-poor zones. The edge of the BSE-zoned area (marked with white lines in Fig. 6) has slightly increased contents of Y and U. Yttrium and Th are found in elevated concentrations also in chaotically zoned interior regions surrounding the primary growth zonation. Other elements detected did not show significant spatial variations.

Spectroscopy

Raman line scans across REE-rich and REE-poor primary growth zones revealed minor variations in spectral positions of Raman bands, not exceeding 13 cm^{-1} ; there are also accompanying minor variations of band shapes and relative intensities. Changes in band positions are particularly noticed in the spectral ranges $800\text{--}1100\text{ cm}^{-1}$ and $500\text{--}600\text{ cm}^{-1}$. An example for accompanying changes in band shapes is the triplet of bands around 430 cm^{-1} . It should be noted that, in spite of ferriallanite-(Ce) contains

Table 2 Ranges of major-element compositions (EPMA results in wt%) of ferriallanite-(Ce) from Nya Bastnäs, in comparison with two allanite-(Ce) reference samples

Sample	Bastnäs	Oßling	Domanínek	Approximate detection limit
N	51	8	5	
SiO ₂	30.16 – 34.21	30.53 – 32.63	34.62 – 39.20	0.03
TiO ₂	b.d.l. – 0.20	b.d.l.	0.29 – 0.39	0.06
UO ₂	b.d.l.	b.d.l.	0.14 – 0.41	0.09
ThO ₂	b.d.l.	b.d.l.	0.72 – 1.38	0.07
Al ₂ O ₃	11.85 – 17.42	17.83 – 21.03	15.58 – 21.34	0.03
Fe ₂ O ₃ *	6.51 – 12.36	b.d.l. – 1.84	b.d.l. – 3.14	0.07
Y ₂ O ₃	0.11 – 0.55	b.d.l. – 0.22	b.d.l. – 0.11	0.06
La ₂ O ₃	4.76 – 8.58	4.64 – 6.21	2.96 – 4.00	0.07
Ce ₂ O ₃	6.86 – 12.57	10.10 – 12.84	6.22 – 8.07	0.09
Pr ₂ O ₃	0.51 – 1.25	1.16 – 1.51	0.61 – 0.79	0.17
Nd ₂ O ₃	1.91 – 3.90	4.02 – 4.61	2.00 – 2.50	0.28
Sm ₂ O ₃	b.d.l. – 0.55	0.35 – 0.63	0.21 – 0.32	0.22
Gd ₂ O ₃	b.d.l. – 0.43	b.d.l. – 0.53	b.d.l. – 0.24	0.18
Tb ₂ O ₃	b.d.l. – 0.16	0.19 – 0.41	b.d.l.	0.10
FeO*	5.55 – 10.82	9.01 – 10.68	3.51 – 8.38	0.07
CaO	9.49 – 16.13	10.94 – 12.43	8.79 – 17.20	0.02
MgO	0.31 – 1.37	0.09 – 0.15	0.18 – 0.97	0.02
MnO	b.d.l. – 0.29	0.19 – 0.41	b.d.l. – 0.12	0.07
Na ₂ O	b.d.l.	b.d.l. – 0.06	b.d.l. – 0.08	0.04
Total**	97.30 – 103.12	94.50 – 97.77	84.22 – 97.20	

N number of point analyses, *b.d.l.* below detection limit

*Fe²⁺/Fe³⁺ ratio was calculated to balance 25 negative charges in total

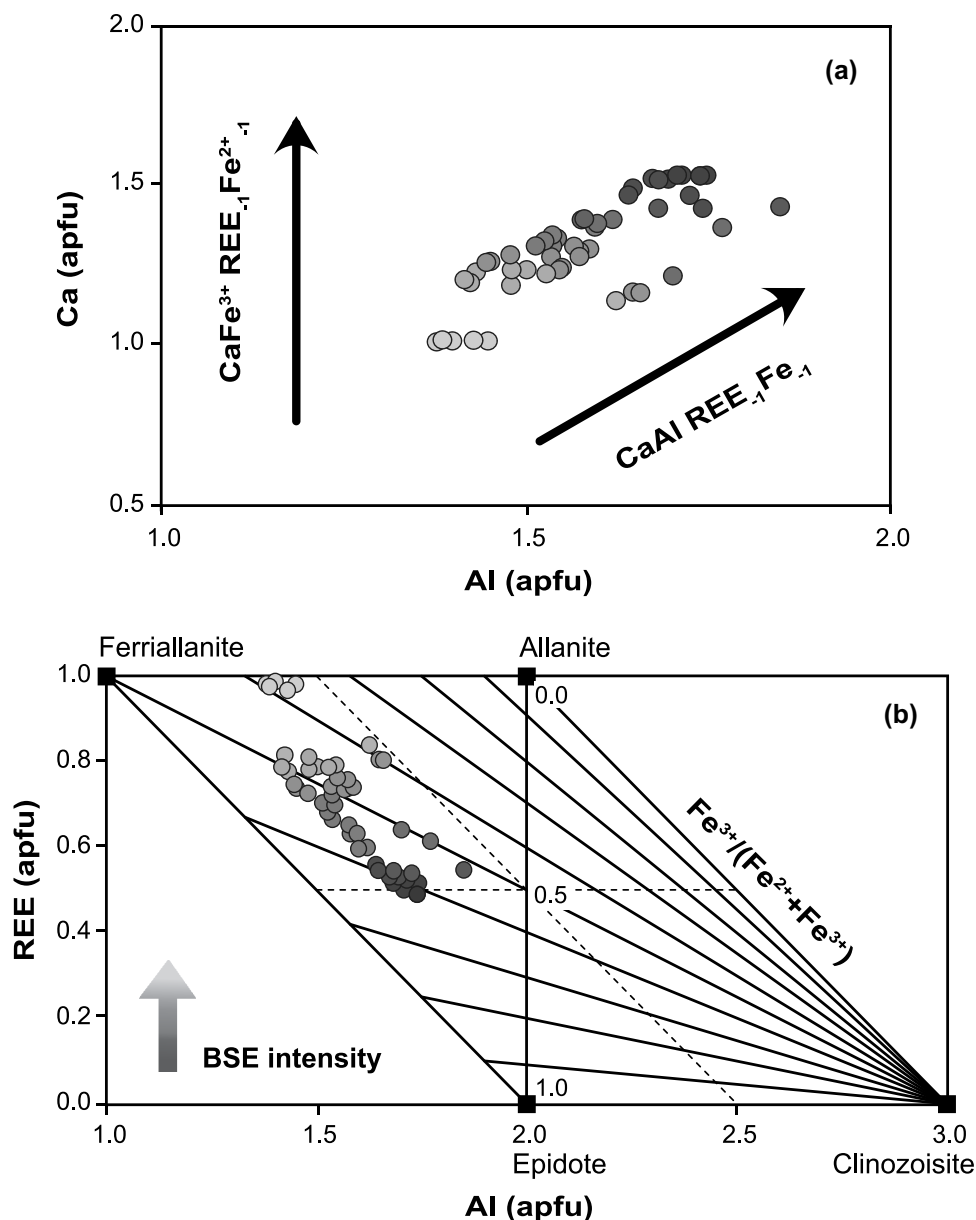
**Low totals are attributed to the small sample size of the acicular crystal from Oßling, and strong radiation damage of the Domanínek sample

OH⁻ groups, no significant O–H stretching signal was detected.

The Raman spectrum of the fragment of ferriallanite-(Ce) that was annealed at 280 °C for 4 days is largely similar to the spectrum of the untreated counterpart (Fig. 7). Both spectra are somewhat similar to the Raman spectrum of fresh allanite-(Ce) from Oßling, Germany. In contrast, metamict allanite-(Ce) from Domanínek, Czech Republic, yielded a notably different Raman spectrum that is typical of glassy silicates, with a weak band around 950 cm^{-1} (Fig. 7).

Untreated and annealed fragments of the sample were also checked for possible luminescence using blue, green, red and near infrared laser excitation. No significant emission was detected.

Fig. 5 Chemical composition of ferriallanite-(Ce) and its variations along the two arrows shown in Fig. 4 with all points (total 51 analyses). **a** Plot of Ca against Al. **b** Plot of REE against Al. Radial lines emanating from the clinozoisite composition allow to estimate the portion of Fe^{3+} in total Fe (central y axis; Petrik et al. 1995). The grey levels of the symbols visualise the observed BSE intensities



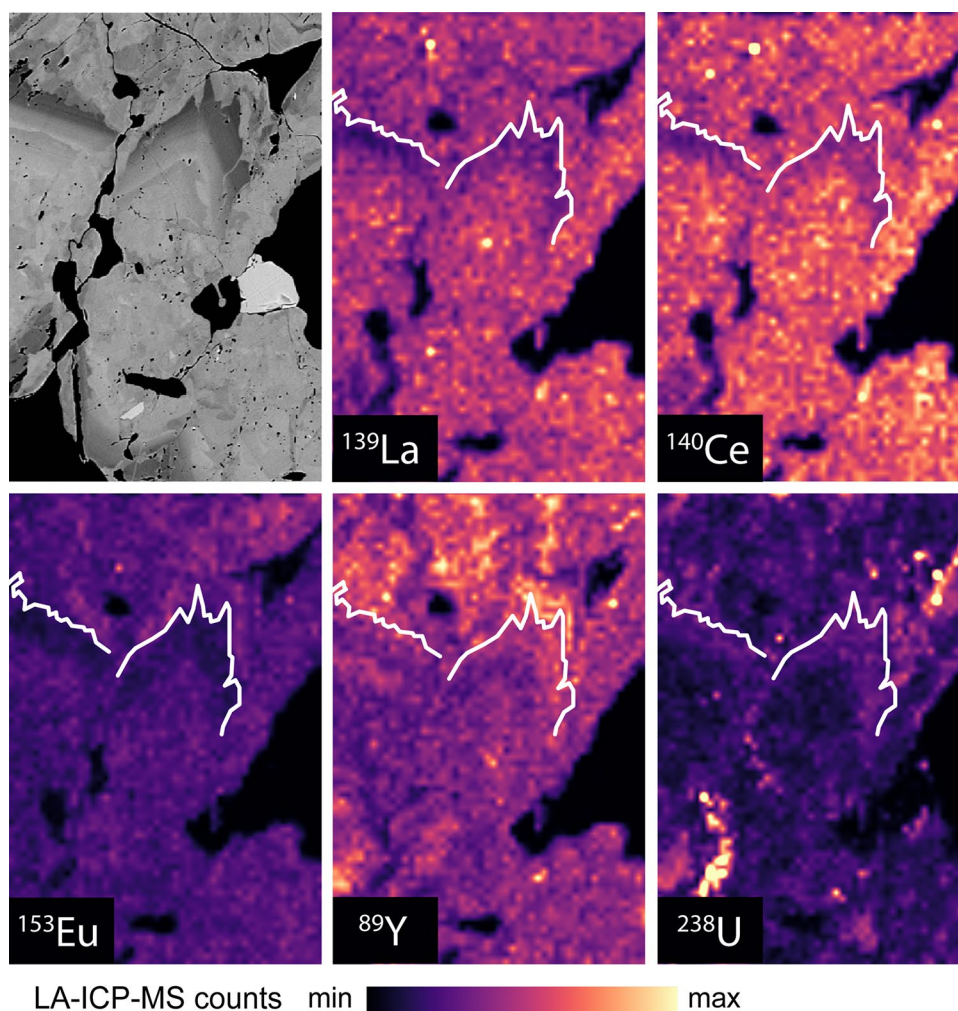
Discussion

Results of chemical analyses of allanite-group minerals were converted to mineral formulae using normalization of the sum of metal cations to 8 and total charge to 25. This approach allows one to estimate the $\text{Fe}^{3+}/\text{Fe}^{2+}$ ratio, under the assumption that there are no A- and M-site vacancies and no “oxy-allanite” component present (Ercit 2002). Analytical totals close to 100 wt% and the virtual absence of elements that are characteristic for altered allanite-group minerals and common in radiation damaged specimens (Na, Pb, P, Ti; Ueda 1955; Deer et al. 1986), we may assume that our sample did not experience significant chemical alteration. This, however, appears to be in contrast to the irregular zoning exhibited by a major part of the sample.

Our sample is much poorer in Mg and REEs and richer in Al, compared to ferriallanite-(Ce) from the Bastnäs deposit studied by Holtstam et al. (2003), which may indicate considerable chemical variability of this mineral.

Ferriallanite-(Ce) yielded Raman spectra that are somewhat similar to the fairly unsharp spectra of ferriallanite-(La) (Varlamov et al. 2019); however, our spectra show much more pronounced and well-defined bands. Spectra depend on chemical compositions of the sample, especially its REEs contents (Fig. 8). Stretching motions in sorosilicates for Si_2O_7 and SiO_4 complexes occur as intense bands above 700 cm^{-1} . These bands belong to the antisymmetric and symmetric stretching vibration of $\text{Si}-\text{O}_b-\text{Si}$ (O_b —bridging oxygens) and of $\text{Si}-\text{O}_{nb}$ (O_{nb} —non-bridging oxygens) and were observed in ferriallanite-(Ce) from 830 to 1100 cm^{-1}

Fig. 6 Trace-element distribution patterns obtained by LA-ICP-MS from strongly zoned ferriallanite-(Ce). As a visual guide, the edge of the BSE-zoned area is marked by a white line. Note that BSE intensity and La and Ce content correlate

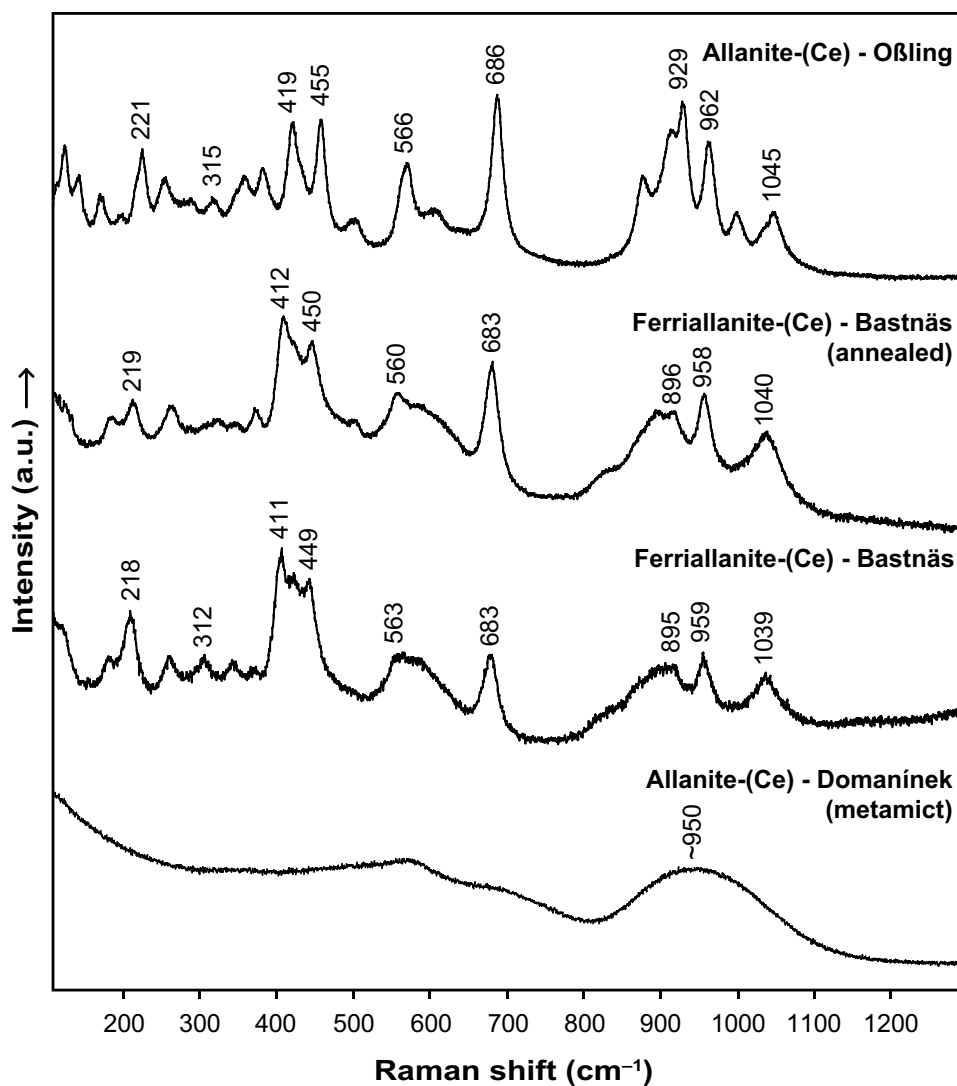


(compare Lazarev 1972; Le Cléac'h and Gillet 1990 or Makreski et al. 2007). According to Chukanov et al. (2014), bands above 1039 cm^{-1} are related to stretching vibrations of the $\text{Si-O}_b\text{-Si}$ depending on the value of the $\text{Si-O}_b\text{-Si}$ angle, where with the increasing angle, the frequency of corresponding vibrations increases as well. Varlamov et al. (2019) discussed that the force characteristics rather than the size of a cation in the A(2) site determine this angle; however, after a thorough examination of the crystal-chemistry of the epidote supergroup minerals, the change in Si1-O9-Si2 angle is related to the M3 octahedral volume rather than the A2-O bond strength (see Bonazzi and Menchetti 1995). This is especially noticeable in REE-bearing epidote supergroup minerals, where the Si1-O9-Si2 angle has lower values due to the entry of larger divalent cations at M3 rather than trivalent cations in A2, and is consistent with our observation of shifts in Raman bands in the $300\text{--}500\text{ cm}^{-1}$ region that are assumed to be assigned to external modes of M-O

interactions (Makreski et al. 2007; see Fig. 9). Bands in the range $550\text{--}700\text{ cm}^{-1}$ were described by Wang et al. (1994) as symmetric stretching of $\text{Si-O}_b\text{-Si}$ bonds.

Annealing of ferriallanite-(Ce) at $280\text{ }^\circ\text{C}$ was mainly done to check for possible annealing-induced spectral changes that, if present, might indicate structural reconstitution of radiation damage. According to Reissner et al. (2019), structural recovery of radiation-damaged allanite-(Ce) is already significant at $280\text{ }^\circ\text{C}$. Annealing at higher temperatures is expected to be more efficient for structural reconstitution; however, potential dehydrogenation and Fe^{2+} oxidation (Janeczek and Eby 1993; Bonazzi and Menchetti 1994; Bonazzi et al. 2009; Reissner et al. 2019) might affect Raman spectra as well and hence bias interpretation. Inconspicuous differences between spectra of untreated and annealed samples (Fig. 7) suggest that radiation damage must be insignificant which is also evidenced by a comparison with the Raman spectrum of a metamict allanite-(Ce) sample from Domanínek. The observation

Fig. 7 Raman spectra obtained from unannealed and annealed chips of the Bastnäs (Sweden) ferriallanite-(Ce), in comparison with spectra of a well-crystallized (Obling, Germany) and a metamict (Domanínek, Czech Republic) allanite-(Ce) reference. Note that spectra of the unannealed and annealed Bastnäs chips are widely similar, which excludes significant annealing-induced structural reconstitution and hence supports the generally low level of radiation damage in this sample

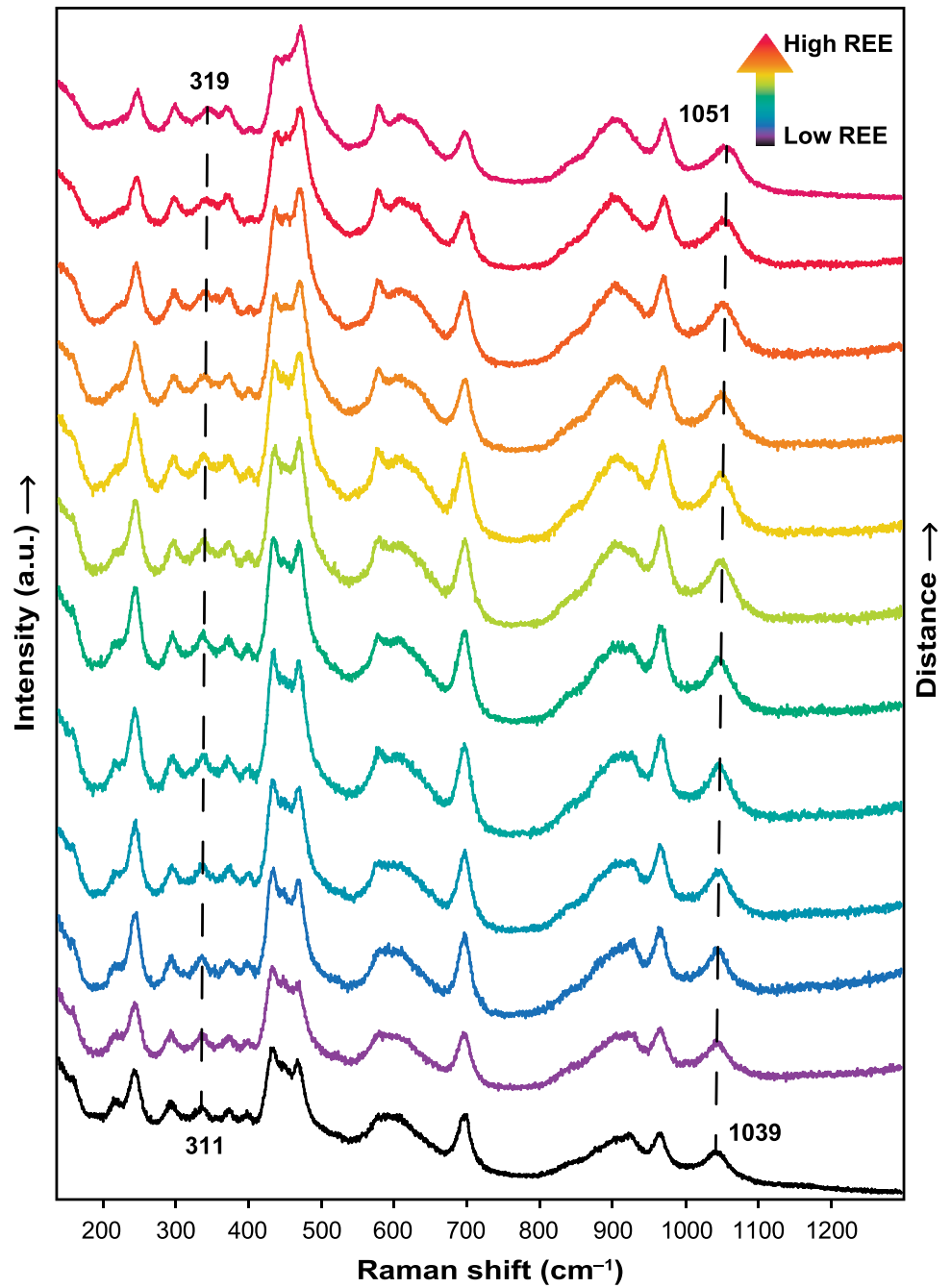


that Raman bands of ferriallanite-(Ce) are generally broader than bands of non-radiation-damaged allanite-(Ce) from Obling (Fig. 7) is assigned to “chemical band broadening” due to more elevated contents of cation substitutions (compare Ruschel et al. 2012). The virtual absence of luminescence, in particular of emissions related to REEs, in spite of significant concentrations of REE³⁺ (Table 2), is explained by quenching, most likely due to elevated concentrations of Fe²⁺ (Pascoal et al. 1999).

As demonstrated in a study of the migration of U and Pb in U-rich minerals (Holá et al. 2021), LA-ICP-MS imaging of individual isotopes can be advantageous in elucidating the evolution of geological processes. This is particularly beneficial for the detection of isotopes of trace elements with

sub-ppm concentrations (Chew et al. 2021), which EPMA is unable to detect. Unfortunately, due to the very small dimensions of the investigated areas of interest and the measured signal-to-noise ratio, our results are merely semi-quantitative. The U and Th content analysed by LA-ICP-MS in ferriallanite-(Ce) from Bastnäs region was reported by Holtstam et al. (2003) as 2.6 ± 0.2 ppm for U and 0.25 ± 0.03 ppm for Th (in total ~3 ppm), which on our estimate according to the low signal intensity (counts per second) should correspond to the same values. Differences in signal intensity in and out of the zonation were observed; however, it is important to highlight the fact that due to a different orientation of the ferriallanite-(Ce) crystal in the studied profile, the material could be ablated differently (Tsibidis et al. 2020).

Fig. 8 Series of 12 Raman spectra obtained along 40 μm line (line 1 in Fig. 4) across zoned ferriallanite-(Ce). Most significant changes in band positions are highlighted by dashed lines



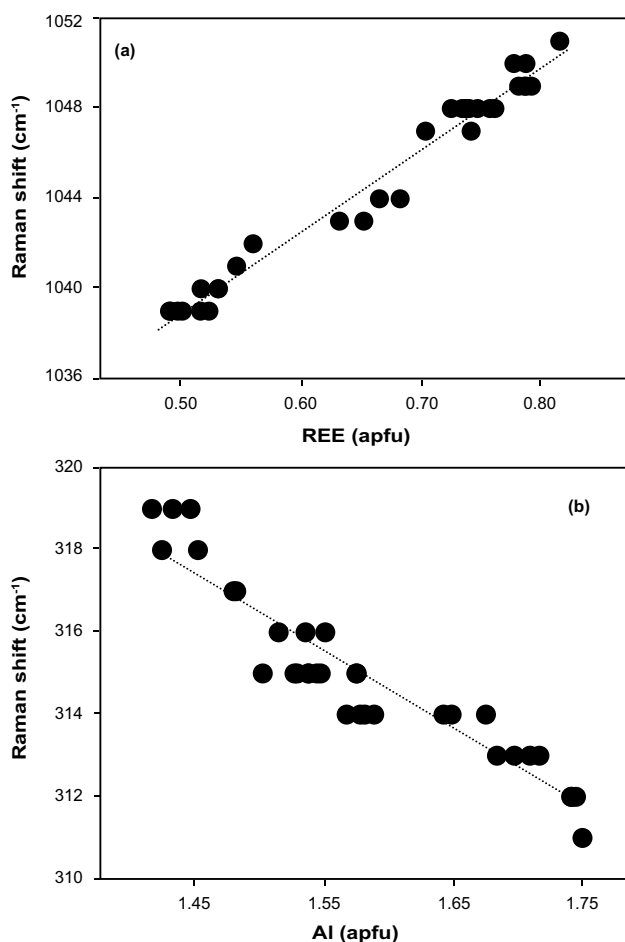


Fig. 9 Comparison of Raman shifts and chemical parameters. **a** Plot of the spectral position of the $\sim 1045\text{ cm}^{-1}$ band (related to the Si–O_b–Si angle; Varlamov et al. 2019) against total REE. **b** Plot of the spectral position of the $\sim 315\text{ cm}^{-1}$ band (related to a M–O external mode; Makreski et al. 2007) against Al. Dotted lines are visual guides

Conclusions

Results of chemical analyses combined with Raman spectroscopy and LA-ICP-MS imaging were found to be useful for studying the crystal chemistry of ferriallanite-(Ce) from Nya Bastnäs, Sweden. Raman spectra for ferriallanite-(Ce) are presented and discussed for the first time. Results of chemical analyses obtained across REE-rich and REE-poor zones show that BSE intensities of the studied ferriallanite-(Ce) correlate with the chemical composition, in particular the Ca/REE ratio. These compositional variations are also reflected in minor differences in Raman spectra and are especially noticeable for bands around the 1045 cm^{-1} that are related to vibrations of the Si–O_b–Si angle. The apparent absence of PL emissions, assigned to Fe²⁺-related quenching in ferriallanite-(Ce), shows that in some allanite-group species, the PL-fingerprinting technique cannot be used.

Supplementary Information The online version contains supplementary material available at <https://doi.org/10.1007/s00710-023-00829-y>.

Acknowledgements We are grateful to Petr Zaunstöck for sample preparation. The authors would like to thank two anonymous reviewers for their comments and constructive suggestions that are highly appreciated. We are also grateful to the Guest Editor Eugen Libowitzky for his suggestions and handling this manuscript.

Funding Open access publishing supported by the National Technical Library in Prague. Financial support was provided by the Project Internal Grant Agency (IGA) of Masaryk University via grant CZ.02.2.69/0.0/0.0/19_073/0016943.

Open Access This article is licensed under a Creative Commons Attribution 4.0 International License, which permits use, sharing, adaptation, distribution and reproduction in any medium or format, as long as you give appropriate credit to the original author(s) and the source, provide a link to the Creative Commons licence, and indicate if changes were made. The images or other third party material in this article are included in the article's Creative Commons licence, unless indicated otherwise in a credit line to the material. If material is not included in the article's Creative Commons licence and your intended use is not permitted by statutory regulation or exceeds the permitted use, you will need to obtain permission directly from the copyright holder. To view a copy of this licence, visit <http://creativecommons.org/licenses/by/4.0/>.

References

- Ahijado A, Casillas R, Nagy G, Fernández C (2005) Sr-rich minerals in carbonatite skarn, Fuerteventura, Canary Islands (Spain). *Mineral Petrol* 84(1):107–127
- Andersson UB (editor) (2004) The Bastnäs-type REE-mineralisations in north-western Bergslagen, Sweden. *Sveriges Geologiska Undersökning Rapporter och Meddelanden* 119:1–34
- Armbruster T, Bonazzi P, Akasaka M, Bermanec V, Chopin C, Gieré R, Heuss-Assbichler S, Liebscher A, Menchetti S, Pan Y, Pasero M (2006) Recommended nomenclature of epidote-group minerals. *Eur J Mineral* 18(5):551–567
- Biagioni C, Bonazzi P, Pasero M, Zaccarini F, Balestra C, Bracco R, Ciriotti ME (2019) Manganiakasakaite-(La) and Ferriakasakaite-(Ce), Two New Epidote Supergroup Minerals from Piedmont, Italy. *Minerals* 9(6):353
- Bonazzi P, Menchetti S (1994) Structural variations induced by heat treatment in allanite and REE-bearing piemontite. *Am Mineral* 79(11–12):1176–1184
- Bonazzi P, Menchetti S (1995) Monoclinic members of the epidote group: effects of the Al \rightleftharpoons Fe³⁺ \rightleftharpoons Fe²⁺ substitution and of the entry of REE³⁺. *Mineral Petrol* 53(1):133–153
- Bonazzi P, Menchetti S (2004) Manganese in monoclinic members of the epidote group: piemontite and related minerals. *Rev Mineral Geochem* 56(1):495–552
- Bonazzi P, Holtstam D, Bindi L, Nysten P, Capitani GC (2009) Multi-analytical approach to solve the puzzle of an allanite-subgroup mineral from Kesebol, Västra Götaland, Sweden. *Am Mineral* 94(1):121–134
- Broska I, Petrík I, Williams CT (2000) Coexisting monazite and allanite in peraluminous granitoids of the Tribec Mountains, Western Carpathians. *Am Mineral* 85(1):22–32
- Chew D, Drost K, Marsh JH, Petrus JA (2021) LA-ICP-MS imaging in the geosciences and its applications to geochronology. *Chem Geol* 229:119917

- Chukanov NV, Krivovichev SV, Pakhomova AS, Pekov IV, Schäfer Ch, Vígasina MF, Van KV (2014) Laachite, $(\text{Ca}, \text{Mn})_{2Zr}2\text{N}_b2\text{TiFe}_{\text{O}_14}$, a new zirconolite-related mineral from the Eifel volcanic region. Germany Eur J Mineral 26(1):103–111
- Čermák J (2013) Mineral assemblage of the pegmatite from Domaníněk at Bystřice nad Pernštejnem (in Czech). Master thesis, MU Brno, 57pp
- Deer WA, Howie RA, Zussman J (1986) Rock-forming minerals, vol 1B. Disilicates and Ring Silicates, 2nd ed. Longman, Harlow GB, 629 pp
- Dollase WA (1969) Crystal structure and cation ordering of piemontite. Am Mineral 54:710–717
- Dollase WA (1971) Refinement of the crystal structures of epidote, allanite and hancockite. Am Mineral 56:447–464
- Dollase WA (1973) Mössbauer spectra and iron distribution in the epidote-group minerals. Z Krist 138:41–63
- Ensterö B (2003) En mineralogisk studie av sulfidparageneser i Nya Bastnäsfalltets lantanidmalm, Riddarhyttan, Bergslagen. Master thesis, Department of Geology, Stockholm University. 51 pp
- Ercit TS (2002) The mess that is “allanite”. Can Mineral 40(5):1411–1419
- Ewing RC (1994) The metamict state: 1993 - the centennial. Nucl Instrum Meth B 91:22–29
- Ewing RC, Chakoumakos BC, Lumpkin GR, Murakami T (1987) The metamict state. MRS Bull 12(4):58–66
- Faltusová V, Vaculovič T, Holá M, Kanický V (2022) Ilaps – python software for data reduction and imaging with LA-ICP-MS. J Anal Spectrom 37(4):733–740
- Franz G, Liebscher A (2004) Physical and chemical properties of the epidote minerals—an introduction. In Liebscher A, Franz G (eds) Epidotes, Rev Mineral Geochem 56, pp 1–82
- Gieré R, Sorensen SS (2004) Allanite and other REE-rich epidote-group minerals. In Liebscher A, Franz G (eds) Epidotes, Rev Mineral Geochem 56, pp 429–493
- Grew ES, Essene EJ, Peacor DR, Su SC, Asami M (1991) Dissakisite-(Ce), a new member of the epidote group and the Mg analogue of allanite-(Ce), from Antarctica. Am Mineral 76:1990–1997
- Holá M, Novotný K, Dobeš J, Kreml I, Wertich V, Mozola J, Kubeš M, Faltusová V, Leichmann J, Kanický V (2021) Dual imaging of uranium ore by Laser Ablation Inductively Coupled Plasma Mass Spectrometry and Laser Induced Breakdown Spectroscopy. Spectrochim Acta Part B At Spectrosc 186:106312
- Holtstam D, Andersson UB, Mansfeld J (2003) Ferriallanite-(Ce) from the Bastnäs deposit, Västmanland. Sweden Can Mineral 41(5):1233–1240
- Holtstam D, Ensterö B (2002) Does the Bastnäs REE deposit in central Sweden belong to the Fe oxide-Cu-U-Au-REE class of ores? Abstract Volume, 25th Nordic Geological Winter Meeting, Reykjavík, Iceland, pp 83
- Holtstam D, Andersson UB, Broman C, Mansfeld J (2014) Origin of REE mineralization in the Bastnäs-type Fe-REE-(Cu-Mo-Bi-Au) deposits, Bergslagen, Sweden. Miner Deposita 49:933–966
- Janeček J, Eby RK (1993) Annealing of radiation damage in allanite and gadolinite. Phys Chem Miner 19(6):343–356
- Kartashov PM, Ferraris G, Ivaldi G, Sokolova E, McCammon CA (2003) Ferriallanite-(Ce), $\text{CaCeFe}^{3+}\text{AlFe}^{2+}(\text{SiO}_4)(\text{Si}_2\text{O}_7)\text{O}(\text{OH})$, a new member of the epidote group: Description, X-Ray and Mössbauer study: Errata. Can Mineral 41(3):829–830
- Kvick KÅ, Pluth JJ, Richardson JW Sr, Smith JV (1988) The ferric iron distribution and hydrogen bonding in epidote: a neutron diffraction study at 15 K. Acta Crystallogr B Struct Sci Cryst Eng Mater 44(4):351–355
- Lazarev AN (1972) Vibrational spectra and structure of silicates. Consultant Bureau, New-York, London, 302 pp
- Le Cléac’h L, Gillet P, (1990) IR and Raman spectroscopic study of natural lawsonite. Eur J Mineral 2:43–53
- Lenz Ch, Nasdala L, Talla D, Hauzenberger Ch, Seitz R, Kolitsch U (2015) Laser Induced REE³⁺ Photoluminescence of Selected Accessory Minerals – An “Advantageous Artefact” in Raman Spectroscopy. Chem Geol 415:1–16
- Makreski P, Jovanovski G, Kaitner B, Gajović A, Biljan T (2007) Minerals from Macedonia: XVIII. Vibrational spectra of some sorosilicates. Vibrational Spectroscopy 44(1):162–170
- Merlet C (1994) An Accurate Computer Correction Program for Quantitative Electron Probe Microanalysis. Microchim Acta 114(1):363–376
- Miyawaki R, Yokoyama K, Matsubara S, Tsutsumi Y, Goto A (2008) Uedaite-(Ce), a new member of the epidote group with Mn at the A site, from Shodoshima, Kagawa Prefecture, Japan. Eur J Mineral 20:261–269
- Momma K, Izumi F (2011) VESTA 3 for three-dimensional visualization of crystal, volumetric and morphology data. J Appl Crystallogr 44:1272–1276
- Nagashima M, Nishio-Himane D, Tomita N, Minakawa T, Inaba S (2013) Vanadoallanite-(La): A new epidotesupergroup mineral from Ise, Mie Prefecture. Japan Mineral Mag 77:2739–2752
- Nasdala L (1993) Mineralvorkommen in den Grauwacken der nördlichen Oberlausitz. Emser Hefte 14(1):2–56
- Nasdala L, Irmer G, Wolf D (1995) The degree of metamictization in zircons: a Raman spectroscopic study. Eur J Mineral 7:471–478
- Nozik YK, Kanepit VN, Fykin LY, Makarov YS (1978) A neutron diffraction study of the structure of epidote. Geochem Int 15:66–69
- Papoutsas A, Pe-Piper G (2015) Variation of REE-hydrothermal circulation in complex shear zones: The Cobecquid Highlands, Nova Scotia. Can Mineral 52:943–968
- Pascoal HB, Pontuschka WM, Rechenberg H (1999) Luminescence quenching by iron in calcium aluminoborate glasses. J Non-Cryst Solids 258(1–3):92–97
- Pautov LA, Khorov PV, Ignatenko KI, Sokolova EV, Nadezhina TN (1993) Khristovite-(Ce), $(\text{Ca}, \text{REE})\text{REE}(\text{Mg}, \text{Fe})\text{AlMnSi}_3\text{O}_{11}(\text{OH})(\text{F}, \text{O})$, a new mineral of the epidote group. Zapiski Vserossiyskogo Mineralogicheskogo Obshchestva 122(3):103–111 (in Russian)
- Peacor DR, Dunn PJ (1988) Dollaseite-(Ce) (magnesium orthite redefined) Structure refinement and implications for F + M²⁺ substitutions in epidote-group minerals. Am Mineral 73(7–8):838–842
- Petrík I, Broska I, Lipka J, Šiman P (1995) Granitoid Allanite-(Ce) Substitution Relations, Redox Conditions and REE Distributions (on an Example of I-Type Granitoids, Western Carpathians, Slovakia). Geol Carpathica 46:79–94
- Reissner CE, Bismayer U, Kern D, Reissner M, Park S, Zhang J, Ewing RC, Shelyug A, Navrotsky A, Paulmann C, Škoda R (2019) Mechanical and structural properties of radiation-damaged allanite-(Ce) and the effects of thermal annealing. Phys Chem Miner 46(10):921–933
- Ruschel K, Nasdala L, Kronz A, Hanchar JM, Töbrens DM, Škoda R, Finger F, Möller A (2012) A Raman spectroscopic study on the structural disorder of monazite-(Ce). Miner Petrol 105:41–55
- Sahlström F, Jonsson E, Högdahl K, Troll VR, Harris C, Jolis EM, Weis F (2019) Interaction between high-temperature magmatic fluids and limestone explains ‘Bastnäs-type’ REE deposits in central Sweden. Sci Rep 9(1):1–9
- Sorensen SS (1991) Petrogenetic significance of zoned allanite in garnet amphibolites from a paleo-subduction zone: Catalina Schist, southern California. Am Mineral 76:589–601
- Tsibidis G, Musée L, Kanaev A (2020) The Role of Crystalline Orientation in the Formation of Surface Patterns on Solids Irradiated with Femtosecond Laser Double Pulses. Appl Sci 10(24):8811
- Ueda T (1955) The crystal structure of allanite, $\text{OH}(\text{Ca}, \text{Ce})_2(\text{Fe}^{\text{III}}\text{Fe}^{\text{II}})\text{Al}_2\text{OSi}_2\text{O}_7\text{SiO}_4$. Mem Coll Sci Univ Kyoto Ser B(2):145–163
- Varlamov DA, Ermolaeva VN, Chukanov NV, Jančev S, Vígasina FM, Plechov YuP (2019) New Data on Epidote-Supergroup Minerals:

- Unusual Chemical Compositions, Typochemistry, and Raman Spectroscopy. *Geol Ore Depos* 61(8):827–842
- Vlach SRF, Gualda GAR (2007) Allanite and chevkinite in A-type granites and syenites of the Graciosa Province, southern Brazil. *Lithos* 97:98–121
- Wang A, Han J, Guo L, Yu J, Zeng P (1994) Database of Standard Raman Spectra of Minerals and Related Inorganic Crystals. *Appl Spectrosc* 48(8):959–968
- Wing B, Ferry JM, Harrison TM (2003) Prograde destruction and formation of monazite and allanite during contact and regional metamorphism of pelites: petrology and geochronology. *Contrib Mineral Petrol* 145(2):228–250
- Zeug M, Vargas RIA, Nasdala L (2017) Spectroscopic study of inclusions in gem corundum from Mercaderes, Cauca, Colombia. *Phys Chem Miner* 44(3):221–233

Publisher's Note Springer Nature remains neutral with regard to jurisdictional claims in published maps and institutional affiliations.